molecules

MDPI

Article

Experimental and Theoretical Studies on Optical Properties of Tetra(Imidazole) of Palladium (II) Phthalocyanine

Abdelmajid Timoumi [1,*,†], Davoud Dastan [2,*,†], Bassem Jamoussi [3], Khaled Essalah [4], Omar Hammed Alsalmi [1], Noureddine Bouguila [5], Henda Abassi [6], Radhouane Chakroun [3], Zhicheng Shi [7] and Ştefan Ţălu [8,*]

1 Department of Physics, Faculty of Applied Science, Umm AL-Qura University, Makkah 715, Saudi Arabia
2 Department of Materials Science and Engineering, Cornell University, Ithaca, NY 14850, USA
3 Department of Environmental Sciences, Faculty of Meteorology, Environment and Arid Land Agriculture, King Abdulaziz University, Jeddah 21589, Saudi Arabia
4 Institut Préparatoire aux Etudes d'Ingénieurs d'El Manar, Unité de Recherche en Sciences Fondamentales et Didactique, Equipe de Chimie Théorique et Réactivité (UR14ES10), Université Tunis El Manar, Tunis 2092, Tunisia
5 Laboratoire de Physique des Matériaux et des Nanomatériaux Appliquée à L'Environnement, Faculté des Sciences, Université de Gabès, Cité Erriadh, Zrig, Gabès 6072, Tunisia
6 Laboratoire de Caracterisations, Applications et Modélisation de Matériaux, Faculte des Sciences de Tunis, Université Tunis El Manar, Campus Universitaire, Tunis 1068, Tunisia
7 School of Materials Science and Engineering, Ocean University of China, Qingdao 266100, China
8 The Directorate of Research, Development and Innovation Management (DMCDI), Technical University of Cluj-Napoca, Constantin Daicoviciu St., 400020 Cluj-Napoca, Romania
* Correspondence: aotemoume@uqu.edu.sa (A.T.); d.dastan61@yahoo.com (D.D.); stefan_ta@yahoo.com (Ş.Ţ.)
† These authors contributed equally to this work.

check for updates

Citation: Timoumi, A.; Dastan, D.; Jamoussi, B.; Essalah, K.; Alsalmi, O.H.; Bouguila, N.; Abassi, H.; Chakroun, R.; Shi, Z.; Ţălu, Ş. Experimental and Theoretical Studies on Optical Properties of Tetra(Imidazole) of Palladium (II) Phthalocyanine. *Molecules* **2022**, *27*, 6151. https://doi.org/10.3390/molecules27196151

Academic Editors: Antonio Monari and Carlos Alemán

Received: 16 August 2022
Accepted: 16 September 2022
Published: 20 September 2022

Publisher's Note: MDPI stays neutral with regard to jurisdictional claims in published maps and institutional affiliations.

Abstract: In this work, the optical properties of tetra(imidazole) of palladium phthalocyanine ($PdPc(Im)_4$) in solution form and thin films on glass and fluorine-doped tin oxide (FTO) substrates were investigated via the thermal evaporation technique. The optical band gap was evaluated by ultraviolet–visible spectroscopy (UV-Vis). The energy band gap values were determined based on the Tauc graph. In addition, time-dependent density functional theory (TD-DFT) was used to simulate the UV-Vis absorption spectrum of the ($PdPc(Im)_4$) molecule in the Dimethyl Sulfoxide (DMSO) solution phase. A good correlation was found between the DFT results and the experimental optical results. The band gap values between the experimental and DFT-simulated values are presented. The energy band gap of ($PdPc(Im)_4$) obtained from the DFT calculations showed that it can be efficiently regulated. Frontier molecular orbitals and molecular electrostatic potentials were also proposed in this work. The surface study of the layers deposited on FTO was considered by atomic force microscopy (AFM) and scanning electron microscopy (SEM), and the results demonstrated good homogeneity covering the entire surface. The SEM image showed a homogeneous distribution of the grains with some spherical or rod-shaped structures and no agglomeration structures. This work rendered a strategy for regulating the energy band gap and compared the experimental observations obtained with theoretical studies, which provides a fundamental insight into the optical band for optoelectronic and thin-film solar cells.

Keywords: $PdPc(Im)_4$; band gap energy; DFT; atomic-scale simulation; thin films

1. Introduction

Recently, numerous efforts have been dedicated to the production and study of several semiconductor materials in film form [1–9]. Metalophthalocyanines (MPcs) are the best significant organic materials that are extensively used in optoelectronic devices such as photoconducting agents [10], photovoltaic devices [11–14], nonlinear optics [15], electrocatalysis [5,16], solar cells [17,18], sensors [19–27], catalysis [5,28], and many others. Many researchers are interested in the study of various materials such as metal-substituted

phthalocyanines (Pcs) [29]. Most of these materials are p-type organic semiconductors. There is considerable interest in the study of these materials because of their low cost, excellent thermal and chemical stability, and being versatile alternatives for the fabrication of thin-film-based devices. Moreover, PdPc exhibits longer exciton diffusion length in comparison with other bivalent metal phthalocyanines, such as ZnPc and CuPc [30]. This property, as well as the strong absorption within the visible spectral range, makes PdPc films a quite useful candidate for photovoltaic applications [31]. It has been assumed in the literature [32] that atmospheric oxygen absorbs at the air/MPc interface and at grain boundaries. It was reported that the formation of charge-transfer complexes by coordination of O_2 to MPc at the air/phthalocyanine interface leads to the formation of oxidized MPc^+ and O^{2-} species and injection of hole charge carriers into the film's bulk [33].

However, there are limited studies on other phthalocyanines, particularly tetra(imidazole) of palladium phthalocyanines ($PdPc(Im)_4$). The element palladium in $PdPc(Im)_4$ has several useful applications [34–36]. Supported by this information, we report the optical study of $PdPc(Im)_4$ that renders features for core system advantages for the applications in photovoltaic devices. In our previous work, we have studied PdPc in thin-film and pellet form [37,38]. A few other references have been reported on the fabrication and characterization of MPc thin films [39–42]. PdPc has been used for organic transistors [43,44], perovskite solar cells [45], and sensors [46–48]. Pcs are organic semiconductors with outstanding electrical features [49]. According to Lokesh et al. [50], the cyclic voltammetric data in DMSO showed that the central metal ion Pd does not undergo a redox process, and the redox behavior observed was mainly due to the macrocyclic ring reduction process. This result confirms the hypothesis of the works of Gould R. D [51] and de Haan A. [52] for the oxidation of the MPc species in MPc^+ by atmospheric oxygen at the interface of air/MPc. The UV-Vis spectrum of phthalocyanine materials is at the origin of the molecular orbitals of the 18π aromatic electronic system [53]. These materials have been considered as electrophotographic materials due to their absorption capacity in the ultraviolet and visible range [54]. Currently, it has been reported that high mobility of $PdPc(Im)_4$ thin films can be achieved by using high substrate heating temperature; the latter directly affects the crystal structure, morphology, and optical properties of the desired film.

The current study showed that the orientation of the grains strongly depends on the nature of the substrate, the thermal annealing temperature, and the deposition technique employed. The electronic structure, excitation process, and molecular interaction have been studied for certain metallic phthalocyanines [55] by the density functional theory (DFT) [56–58] and time-dependent DFT (TD) [59]. Herein, we studied the energy band gap of the palladium phthalocyaninein DMSO solution and in thin-film forms using the UV-Vis absorption spectrum technique. Additionally, DFT calculations were used to calculate the E_g (gap) between molecular orbitals of the main peaks of IN spectra and the frontier highest occupied molecular orbital (HOMO) and lowest unoccupied molecular orbital (HOMO-LUMO). Optimized geometry for the $PdPc(Im)_4$ molecule and other detailed quantitative information with electronic structure calculations are also given.

2. Experimental and Theoretical Studies

2.1. Synthesis Method and Deposition of Thin Films

For the synthesis, we used 5 g (0.039 mole) of phtalonitrile mixed with 1.77 g (0.01 mole) of palladium acetate in DMAE with 1 mL of DBU at 140 °C. Then, the mixture was stirred for 2 h at 180 °C. Subsequently, the product was cooled at room temperature and filtered. The obtained solid was finely ground and washed successively with methanol, hot alcohol, and water to remove intermediates and unreacted components. Then, the compound was purified in Bio-Beads using chloroform. The final product obtained was bluish-green in color. The latter was dried in an oven for 1 h and subsequently prepared using the thermal evaporation technique. Evaporation was carried out using resistive heating of about 20 mg of the material in tungsten boat under a vacuum of 5×10^{-6} Torr. The boat was heated by

passing a high current (100 A). The obtained layers on a clean glass and FTO substrates were homogeneous and had a thickness of approximately 0.1 μm.

2.2. Characterization

The absorption spectra were measured using a UV-Vis spectrometer (Shimadzu) with a resolution of 0.1 nm. The optical band gap was estimated using equation (1) and according to the Planck formula as follows [60–65]:

$$E_g = \Delta E = \frac{hc}{\lambda} \quad (1)$$

where h is the Planck constant (6.62617×10^{-34} J·s), c is the velocity of light (2.9979×10^{8} m/s), and λ represents the absorption limit wavelength (nm), achieved from the onset of the absorption graph [60–65]. The visualization of the surface morphology of the layers was done using atomic force microscopy (AFM, Veeco CP-II) in contact mode with a scanning frequency of 1 Hz and points in Si and Shimadzu-type scanning electron microscopy (SEM, Superscan SSX-550). The synthesis product purity was verified by 1H NMR (Varian XL-200 NMR spectrometer, DMSO d6), elemental analysis (Costech ECS 4010 instrument), and MS and MS-MS spectra (Thermo Quantum Access Mass spectrometer with H-ESI probe conducted in positive ion mode). The analyses were as follows: 1H NMR (DMSO): d, ppm 8.05–8.12(4H, s, broad), 7.71–7.75 (4H, s, broad), 7.4–7.6 (4H, s, broad), and 7.15–7.46(16H, d, broad). Anal. ($C_{44}H_{24}N_{16}Pd$): C, 59.84; H, 2.74; N, 25.37; Pd, 12.05; found: C, 59.40; H, 3.03; N, 25.82; MALDITOF-MS m/z: calculated 882.14; found + 883.3 (M + 1).

2.3. Theoretical Calculations

DFT calculations were performed with Gaussian09w [56,58,66,67] using the functional B3LYP-GD3 with Grimme's dispersion correction [68] and the SDD basis set [69]. The effect of the DMSO solvent on ($PdPc(Im)_4$) was calculated by the SMD model [70]. To study the UV spectra, we used the TD-DFT method on the optimized structure in the DMSO solvent using the same level of theory (B3LYP-GD3/SDD and SMD to simulate the DMSO effect). In addition, we determined the energy of the molecular orbitals and then evaluated the optical gap energy (E_g) (difference between the HOMO and the LUMO border orbitals and between the molecular orbitals of the main peaks of the spectrum). The $PdPc(Im)_4$ structure was optimized using the B3LYP-GD3 function. Frequency calculations were performed to identify the nature of the stationary points.

3. Results and Discussion

3.1. The Optimized Molecular Structure

Figure 1a depicts the optimized molecular structure of the $PdPc(Im)_4$ polymer which shows a square-planar-type configuration with a metal ion at the center (Pd). N atoms are marked in blue; C atoms are in gray. The average Pd–N bond length of the four Pd-N bonds of the optimized structure was 2.006 Å. Figure 1b illustrates the M-plan structure of the PdPc molecule. Figure 1c,d presents distances and angles between atoms in the $PdPc(Im)_4$ molecule. Technically speaking, N1 and N2 are the pyrrole and meso positions of nitrogen, respectively. C1 and C2 are the alpha and beta positions of the carbon. The positions, which are of significant interest, are the meso position of the nitrogen that varies with analogous molecules and the position of the nitrogen pyrrole due to the direct bond with the central atom of palladium.

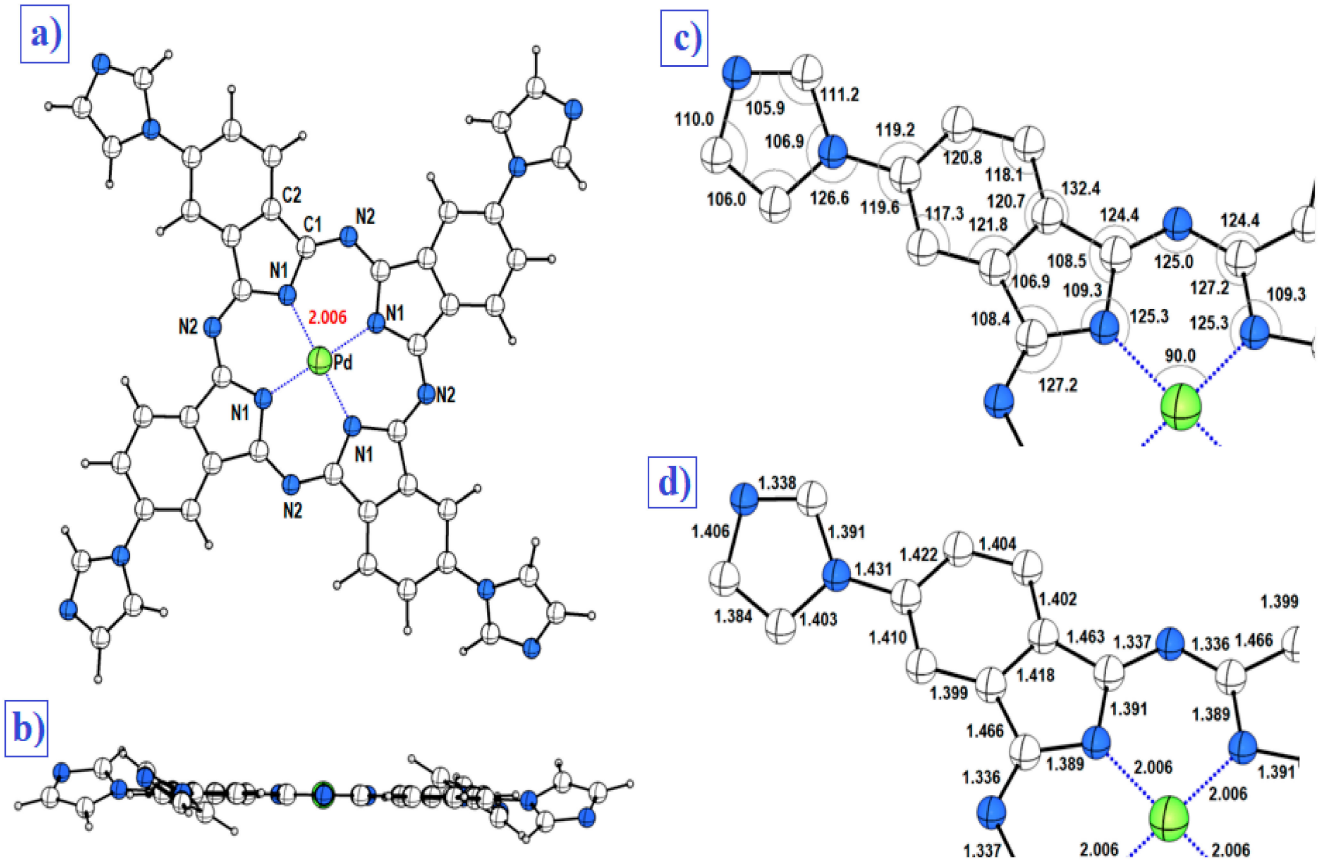

Figure 1. (**a**) Chemical structure of the singlet stat of the neutral PdPc(Im)4 Ci symmetric molecule calculated at the B3LYP-D3/SDD level of theory, taking into account the effect of the DMSO solvent with the SMD model, (**b**) plan structure of the optimized PdPc(Im)4 molecule, (**c**) distances in Å on a quarter (1/4) magnification of the PdPc(Im)4 molecule (all hydrogen atoms have been omitted for clarity of the figure), and (**d**) angles between atoms in degrees represented on a quarter of the molecule for more clarity (all hydrogen atoms have been omitted for clarity of the figure).

3.2. The Frontier Molecular Orbitals (FMOs)

The LUMO and the HOMO mainly form the frontier molecular orbitals (FMOs). The FMOs are very important for studying the chemical and electrical features of substrates [71]. They impact material properties through the development of their polarities and the abilities for absorbing light. On the other hand, they function as acceptor and donor orbitals [72]. Figure 2 presents the computational study based on the density functional theory (DFT) and time-dependent DFT (TD-DFT). This study was carried out to better understand the geometric and photophysical properties of PdPc(Im)$_4$. It describes the HOMO and LUMO electron density, the optimized molecular structures, and the isosurfaces of PdPc(Im)$_4$. The apparent plane geometries, the largely delocalized LUMO and HOMO electron densities, and the existence of π and σ orbitals in the FMOs are favorable to the processes of electron migration between these macrocycles. In addition, the related density of state calculations of the PdPc(Im)$_4$ was studied in DMSO solution, which presents the virtual and occupied orbitals.

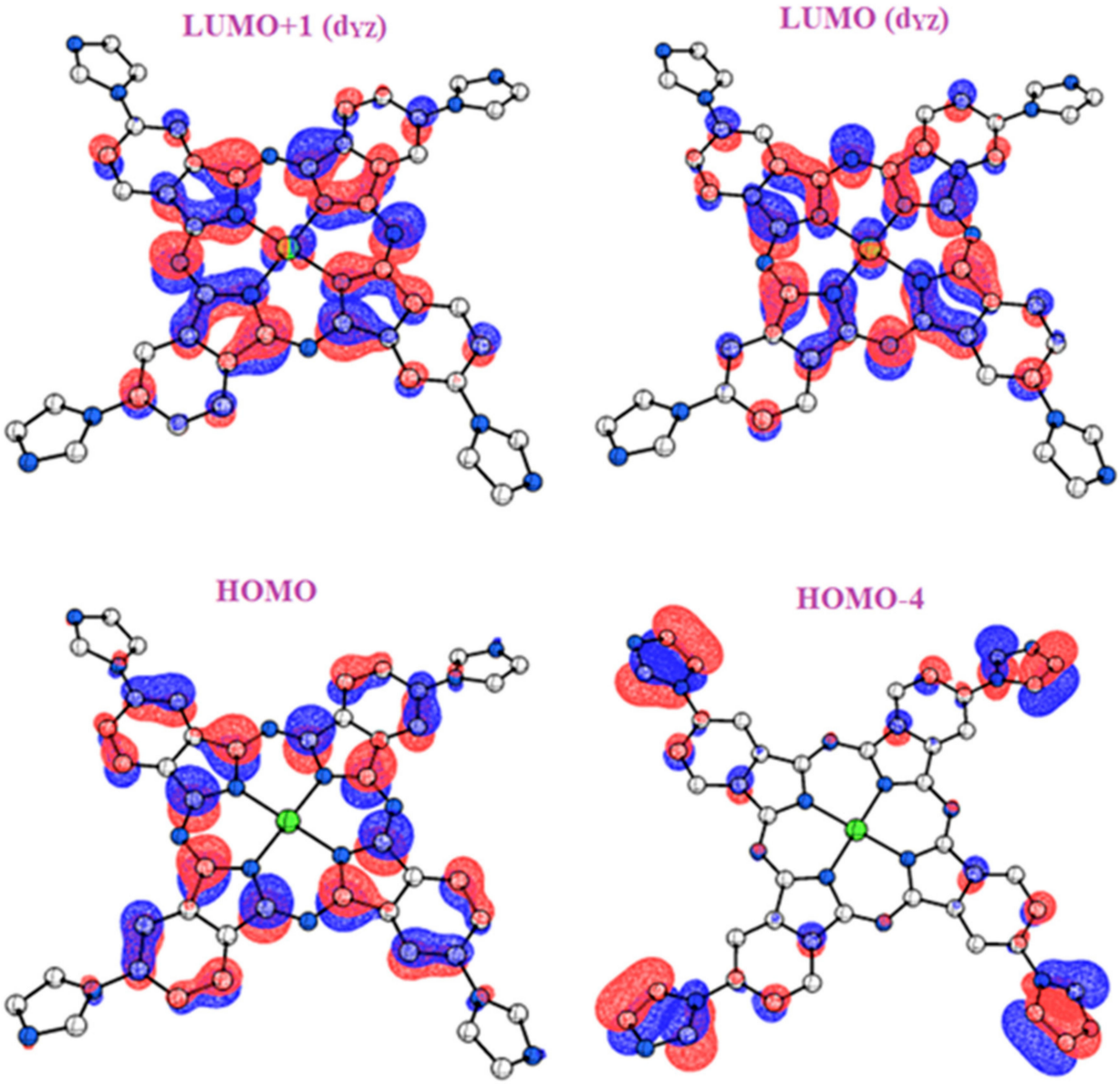

Figure 2. OMs that contribute to UV transitions. Contour plots (contour value = 0.025) of HOMO-n and LUMO + n of $PdPc(Im)_4$ calculated at the B3LYP-D3/SDD level of theory in DMSO. LUMO and LUMO + 1 are degenerate.

3.3. Molecular Electrostatic Potentials

Molecular electrostatic potentials (MEPs) are very beneficial for studying the relationship between physicochemical features and its molecular structure. This is done by visualization of molecular size and shape, as well as by the charge distribution in the molecule in terms of color calibration [73]. Figure 3 depicts the electrostatic potential surface (EPS) and contours of $PdPc(Im)_4$ from the total self-consistent field (SCF) density and mapped with ESP. Figure 4 presents electrostatic potential surface and contours of $PdPc(Im)_4$ from the total SCF density in the plan of a molecule and a cross-section in terms of that mapped with electrostatic potential from the total SCF density and contour map on N and Pd atoms. The electrostatic potential surfaces generally render information regarding the stacking of $PdPc(Im)_4$ molecules in the sample at the nano-scale. The possible agglomeration in the sample is the H atom, which is owing to a high-energy change in the absorption graph as well as details given by the distribution of electrostatic potential on the molecule.

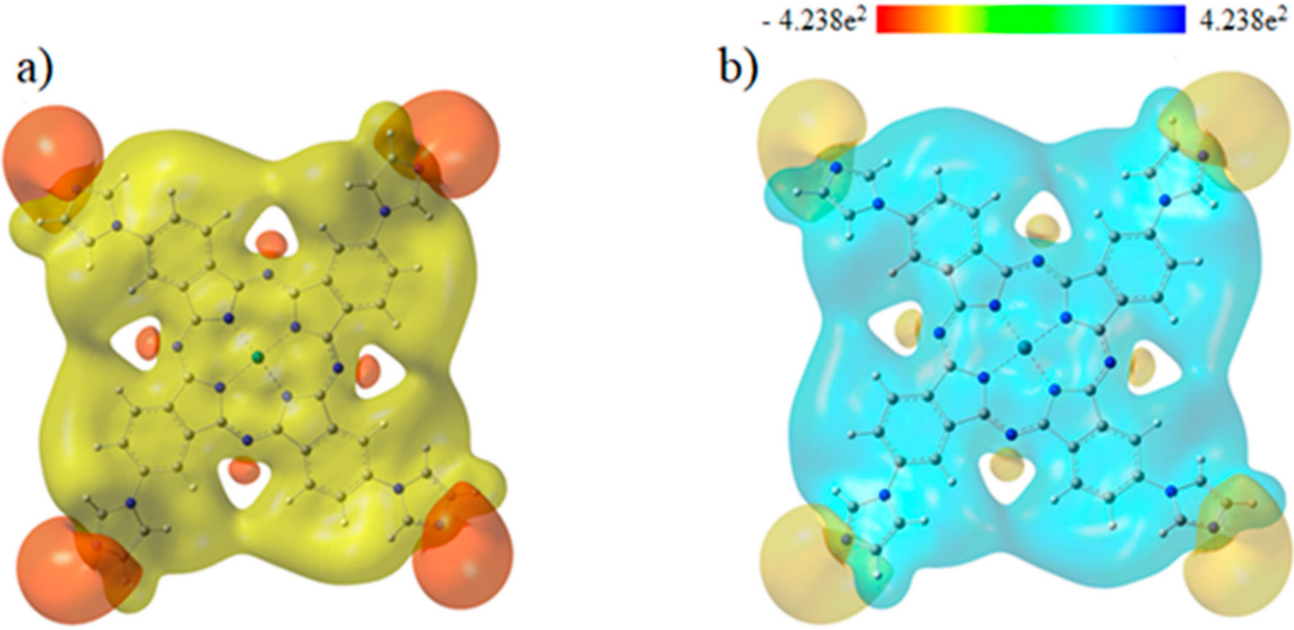

Figure 3. Electrostatic potential surface and contours of PdPc(Im)4: (**a**) from total SCF density (isoval = 0.025); (yellow = positive, orange = negative) and (**b**) mapped with ESP.

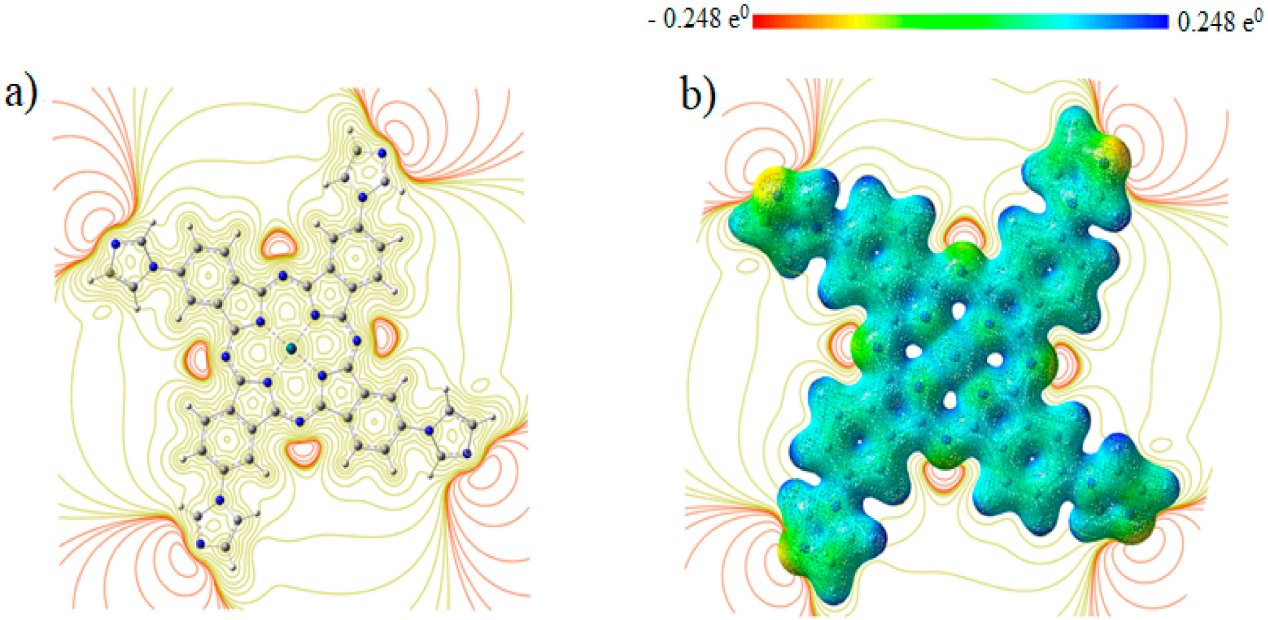

Figure 4. (**a**) Electrostatic potential surface and contours of PdPc(Im)4 from total SCF density (isoval = 0.025) in the plan of molecule (yellow = positive, orange = negative) and (**b**) a cross-section in terms of that mapped with electrostatic potential from total SCF density and contour map.

The surface map of the molecular electrostatic potential (MEP) was calculated and is shown in Figure 5. This map shows the existence of four possible sites of electrophilic attack, and it is neutral on the conjugate ring. The region near the central atom of the molecule (Pd) is positive because the carbon atom (C) is surrounded by electropositive atoms. The findings demonstrate that the site including nitrogen atoms are the most reactive site of the PdPc(Im)$_4$ molecule. These sites provide details related to the region wherein the compound have intermolecular interplays. The behavior of ESP on the phthalocyanine ring is also related to the magnetic separation and position of chemical shift in C-NMR [74,75].

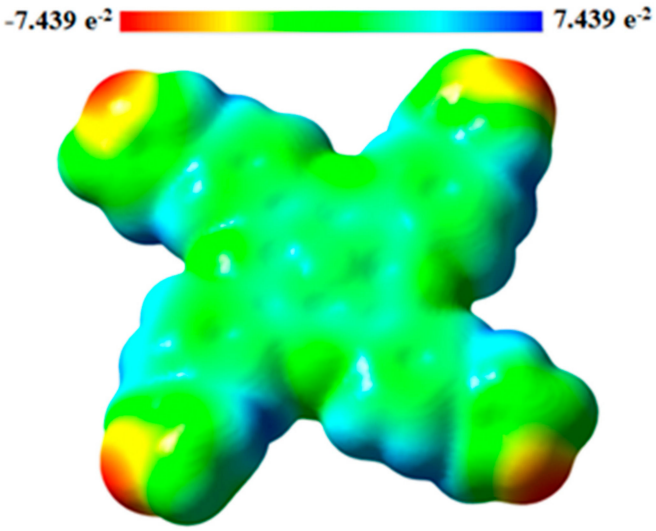

Figure 5. Molecular electrostatic potential (MES) surface for PdPc.

3.4. Optical Absorption Analysis

The optical absorption spectra were made in the wavelength range between 300 and 900 nm using a UV–visible spectrometer. In fact, n→π* and π→π*-type electronic transitions in π-conjugated organic compounds result in a UV-Vis absorption graph [76]. These transitions are usually owing to movements of electrons among boundary molecular orbitals (FMOs). In addition, organic molecules of phthalocyanine and their compounds exhibit optical features due to their cyclic structure. These compounds possess two different types of energy bands including the Q band (a porphyrin band) and the B band (c or Soret band). The peaks observed in the region of the Q band cited in the 610-680 nm range are responsible for the observed green color of this synthesized complex (Figure 6). These transitions can also be attributed to π–π* transitions. Figure 7 shows the UV-Vis absorption spectra for $PdPc(Im)_4$ in DMSO solution and thin-film form. For $PdPc(Im)_4$ dissolved in DMSO, Figure 7a illustrates a first absorption peak at 350 nm (band B) in the visible spectrum region. A less intense shoulder peak around 610 nm corresponds to the dimer of the phthalocyanine, and a peak at 650 nm to the Q band absorption [77]. Figure 7b depicts the UV-Vis spectrum of $PdPc(Im)_4$ thin film. It shows a typical Soret band at around 340 nm, which corresponds to π→π* transition. Furthermore, the band located in the range of 600–680 nm corresponds to Q bands, which was assigned to the dimer of phthalocyanines. ($PdPc(Im)_4$) molecules can interact with each other through delocalized π electrons and hydrogen bonds.

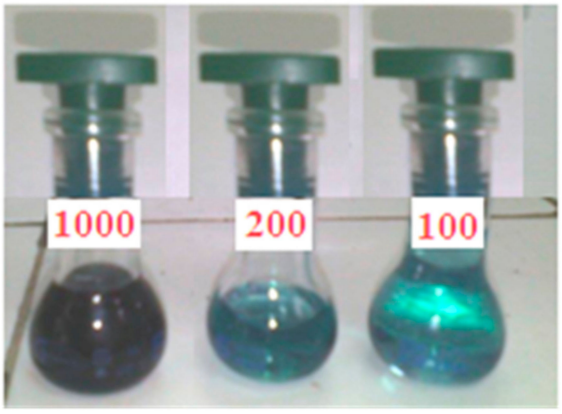

Figure 6. Color of complex at different concentrations (100 mg·L^{-1}~1.6 × 10^{-4} M; 200 mg·L^{-1}~3.2 × 10^{-4} M; 1000 mg·L^{-1}~1.6 × 10^{-3} M).

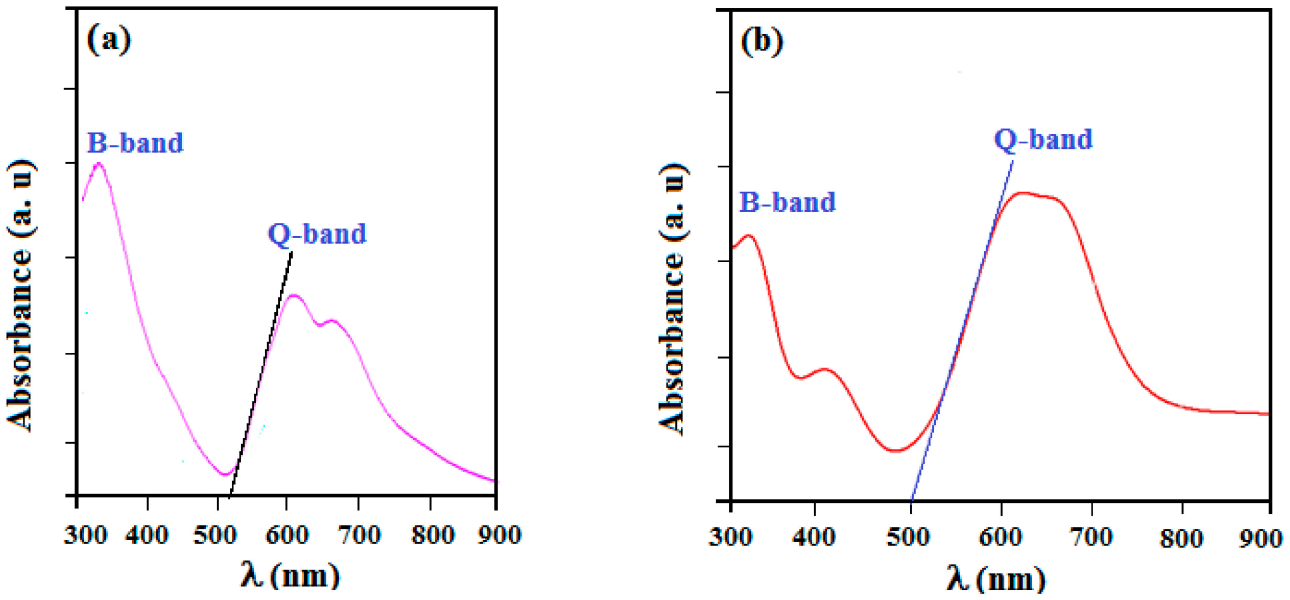

Figure 7. Electronic absorption spectra of $PdPc(Im)_4$ in DMSO solution (10^{-5} M) (**a**) and (**b**) thin-film forms.

The optical band gaps of the $PdPc(Im)_4$ in DMSO solution and thin-film form are also deduced from the figures, which were about 2.41 and 2.48 eV, respectively. The bandgap energy and threshold wavelength were determined using DFT data. The absorption spectrum obtained from the DFT calculations of $PdPc(Im)_4$ in the DMSO solvent is presented in Figure 8. The values of energy bandgaps obtained from experimental graphs, theoretical data, and threshold wavelengths are summarized in Table 1. In the Q band, the electronic transition occurred from the electron density centered on the phthalocyanine (HOMO) molecule to the low electron density on the Pd-N bond (LUMO) as demonstrated in Figure 8. The evaluated optical energy was about 2.23 eV. The theoretical optical transition obtained by the TD-DFT calculation is in accordance with that determined experimentally [78]. Recognizable functionality groups of palladium phthalocyanine can be deduced depending on the position of the peak and the intensity of the infrared spectrum. Figure 9 demonstrates the IR spectrum obtained from the DFT method and experimental analysis. A large peak was obtained in the 3100-3500 cm^{-1} range due to the stretch band between O-H and N-H [79–85]. The peaks are the signals of OH, CH_2, and C-O [74–77]. In Figure 9, additional peaks observed at 2200 and 3100 cm^{-1} were assigned to C=N and N-H, which are the characteristic signals of palladium phthalocyanine. For $PdPc(Im)_4$ films deposited on FTO, the band gap energy was evaluated based on the study of the absorption graph and the graph described by Tauc [86]. In the literature [87], the obtained band gap energy related to direct transitions in the material is 3.62 eV. The SEM images in Figure 10a shows the morphology of the $PdPc(Im)_4$ on the FTO. It is seen that surface was homogenous and composed of grains with a size between 150 and 200 nm. The three-dimensional AFM image in Figure 10b revealed that the $PdPc(Im)_4$ layer deposited on FTO caused surface smoothening with spherical grains of different sizes and shapes.

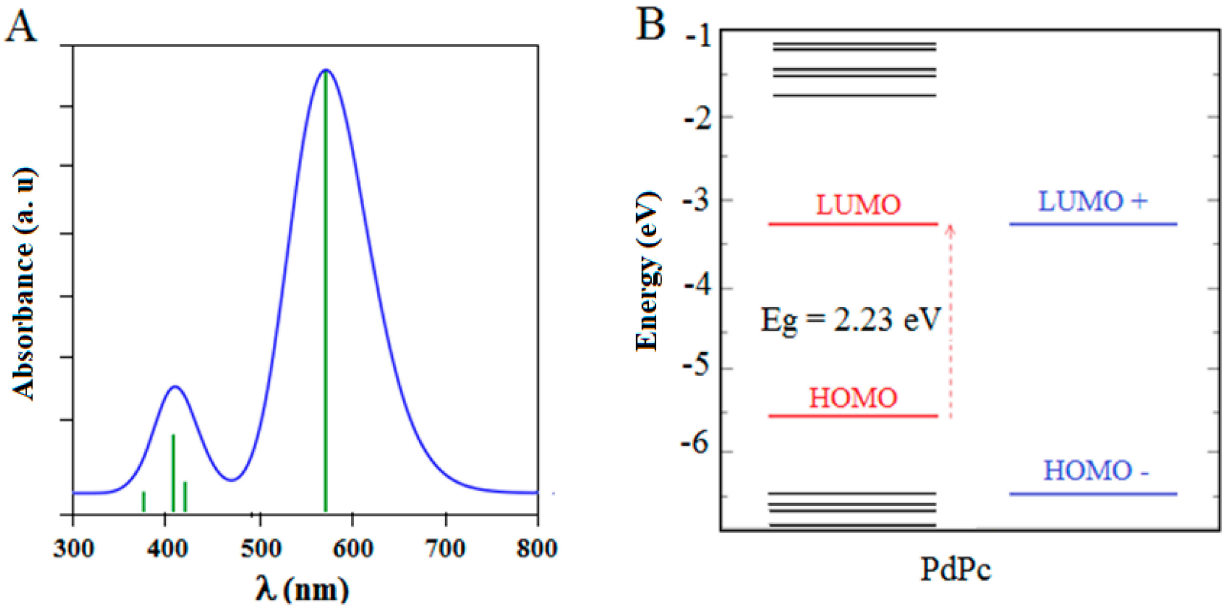

Figure 8. (**A**) Variation of absorbance using DFT and (**B**) $PdPc(Im)_4$ molecular orbital energies in eV. The levels to the right show degenerate energies.

Table 1. Band gap and threshold wavelengths value for $PdPc(Im)_4$ in DMSO solution, $PdPc(Im)_4$-thin films, and $PdPc(Im)_4$-DFT.

	Q-Band	
Material	**Wavelength (nm)**	**E_g (eV)**
$PdPc(Im)_4$ in DMSO solution	515	2.41
$PdPc(Im)_4$-thin films	500	2.48
$PdPc(Im)_4$-DFT	490	2.23

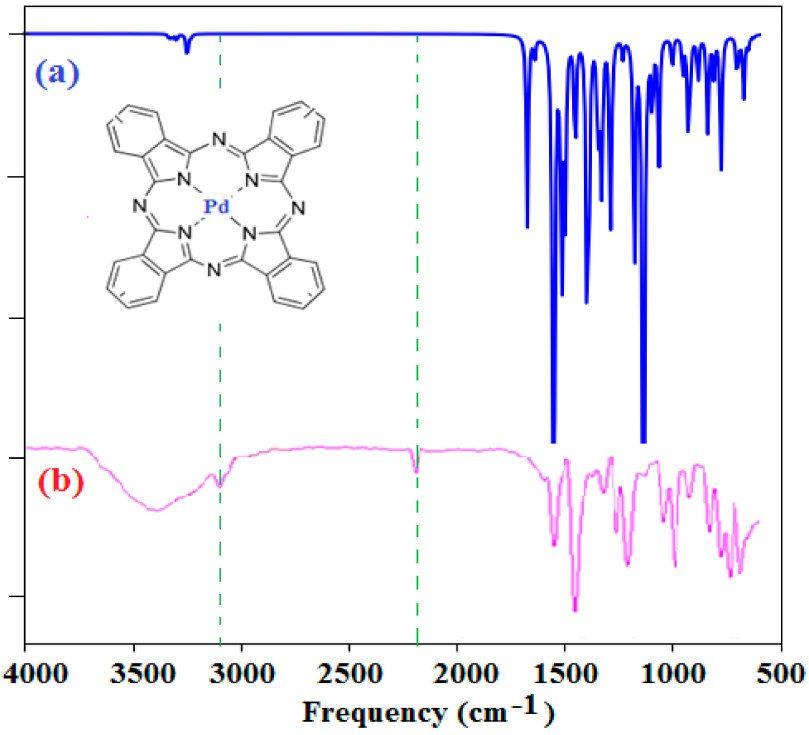

Figure 9. (**a**) Theoretical and (**b**) experimental infrared spectra.

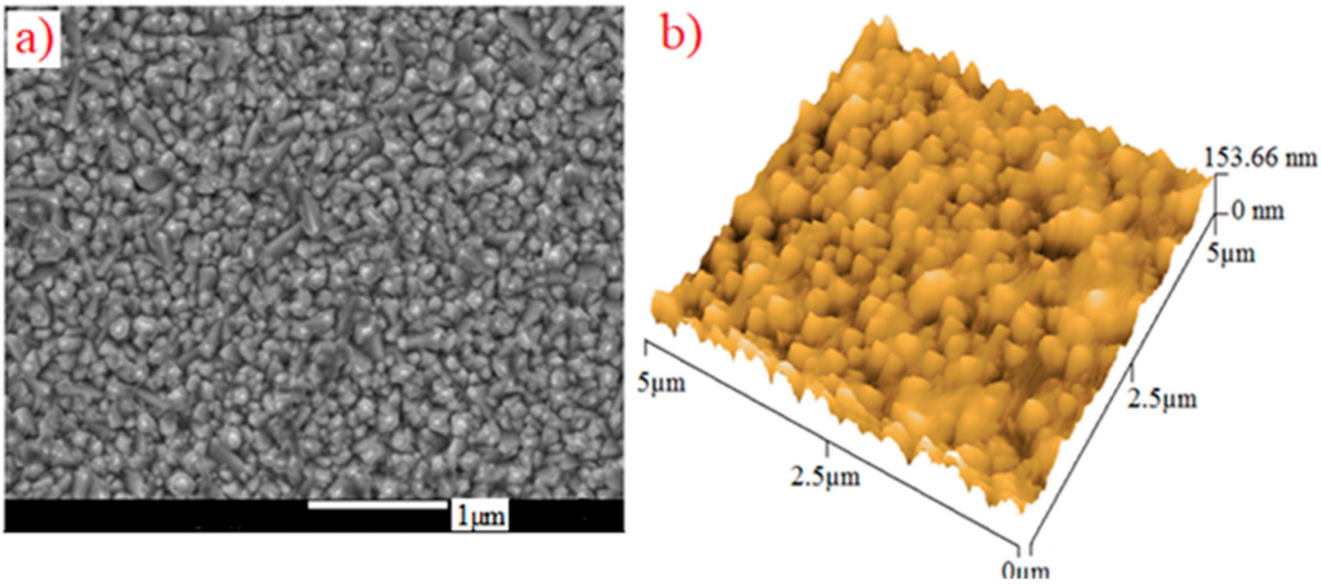

Figure 10. (**a**) SEM analysis and (**b**) three-dimensional AFM analysis of PdPc(Im)4 deposited on FTO by vacuum thermal evaporation technique.

4. Conclusions

In summary, the $PdPc(Im)_4$ in DMSO solution and thin films deposited on glass and FTO by thermal evaporation were prepared. The UV-Vis technique was employed to establish the optical bandgap of the $PdPc(Im)_4$. The optical results demonstrated a band gap of 2.41 eV for the $PdPc(Im)_4$ in the DMSO solution and values of 2.48 and 3.62 eV for the thin layers of $PdPc(Im)_4$ Pc deposited on glass and FTO, respectively, using a Tauc route. MEP analysis was used to identify electrophilic and nucleophilic sites in the molecule as well as to provide additional information about regions of intermolecular interaction. DFT calculations using the DFT-B3LYP method were also used to calculate the band gap of the $PdPc(Im)_4$ molecule, and the achieved bandgap was 2.23 eV, which is close to the experimentally obtained value. The simulated UV-Vis domains are consistent in the shape and position of band B with those of the experimentally obtained results. This study of the $PdPc(Im)_4$ band gap is fundamental for various appliances such as organic photovoltaic devices and light-emitting diodes.

Author Contributions: Conceptualization, methodology, and writing—original draft, A.T.; conceptualization, writing—reviewing and editing, data curation, formal analysis, and supervision, D.D.; investigation, resources, and software, B.J.; investigation and resources, K.E.; resources and validation, O.H.A.; software and resources, N.B.; investigation and resources, H.A.; software and validation, R.C.; investigation, resources, and visualization, Z.S.; resources, software, funding acquisition, and project administration, Ș.Ț. All authors have read and agreed to the published version of the manuscript.

Funding: This research received no external funding.

Institutional Review Board Statement: Not applicable.

Informed Consent Statement: Not applicable.

Data Availability Statement: The data used to support the findings of this study are available from the corresponding authors upon request.

Acknowledgments: The authors would like to thank the Deanship of Scientific Research at UmmAl-Qura University for supporting this work by grant code: (22UQU4331172DSR05).

Conflicts of Interest: The authors declare no conflict of interest.

Sample Availability: Further details about the samples investigated in this study are available upon request from the authors.

References

1. Yin, P.; Shi, Z.; Sun, L.; Xie, P.; Dastan, D.; Sun, K.; Fan, R. Improved breakdown strengths and energy storage properties of polyimide composites: The effect of internal interfaces of C/SiO_2 hybrid nanoparticles. *Polym. Compos.* **2021**, *42*, 3000–3010.
2. Altaf, F.; Ahmed, S.; Dastan, D.; Batool, R.; Rehman, Z.U.; Shi, Z.; Hameed, M.U.; Bocchetta, P.; Jacob, K. Novel sepiolite reinforced emerging composite polymer electrolyte membranes for high-performance direct methanol fuel cells. *Mater. Today Chem.* **2022**, *24*, 100843. [CrossRef]
3. Ashraf, I.; Ahmad, S.; Dastan, D.; Wang, C.; Garmestani, H.; Iqbal, M. Fabrication of ionic liquid based D-Ti_3C_2/MoO_3 hybrid electrode system for efficient energy storage applications. *Electrochim. Acta* **2022**, *429*, 141036.
4. Zhang, W.; Zhu, X.; Liang, L.; Yin, P.; Xie, P.; Dastan, D.; Sun, K.; Fan, R.; Shi, Z. Significantly enhanced dielectric permittivity and low loss in epoxy composites incorporating 3d W-WO_3/$BaTiO_3$ foams. *J. Mater. Sci.* **2021**, *56*, 4254–4265.
5. Alsulamei, A.; Timoumi, A. Tailoring the physical and optical properties of Sn-doped In_2S_3 thin films obtained using VTE technique. *Opt. Mater. X* **2022**, *15*, 100176.
6. Ashraf, I.; Ahmad, S.; Nazir, F.; Dastan, D.; Shi, Z.; Garmestani, H.; Iqbal, M. Hydrothermal synthesis and water splitting application of d-Ti3C2 MXene/V2O5 hybrid nanostructures as an efficient bifunctional catalyst. *Int. J. Hydrog. Energy* **2022**, *47*, 27383–27396.
7. Fathinezhad, M.; AbbasiTarighat, M.; Dastan, D. Chemometrics heavy metal content clusters using electrochemical data of modified carbon paste electrode. *Environ. Nanotechnol. Monit. Manag.* **2020**, *14*, 100307.
8. Alamoudi, E.; Timoumi, A. The synthesis and the effect of Cu on optoelectronic qualities of β-In_2S_3 as a window layer for CIGS thin film solar cells. *Results Phys.* **2022**, *40*, 105858. [CrossRef]
9. Wei, S.; Shi, Z.; Wei, W.; Wang, H.; Dastan, D.; Huang, M.; Shi, J.; Chen, S. Facile preparation of ultralight porous carbon hollow nanoboxes for electromagnetic wave absorption. *Ceram. Int.* **2021**, *47*, 28014–28020.
10. Law, K.Y. Organic photoconductive materials: Recent trends and developments. *Chem. Rev.* **1993**, *93*, 449. [CrossRef]
11. Anthopoulos, T.D.; Shafai, T.S. Influence of oxygen doping on the electrical and photovoltaic properties of Schottky type solar cells based on α-nickel phthalocyanine. *Thin Solid Film.* **2003**, *441*, 207–213.
12. Yin, X.; Zhou, W.; Dastan, D.; Li, J.; Tan, X.; Liu, Y.; Gao, X.; Ma, X. Selectivity sensing response of ZnO-xCo_3O_4 based sensor to CO against CH_4. *Mater. Sci. Semicond. Processing* **2022**, *149*, 106883. [CrossRef]
13. Schueppel, R.; Timmreck, R.; ALllinger, N.; Mueller, T.; Furno, M.; Uhrich, C.; Leo, K.; Riede, M. Controlled current matching in small molecule organic tandem solar cells using doped spacer layers. *J. Appl. Phys.* **2010**, *107*, 044503.
14. Yin, X.; Li, J.; Wang, Q.; Dastan, D.; Shi, Z.; Alharbi, N.; Garmestani, H.; Tan, X.; Liu, Y.; Ma, X. Opposite Sensing Response of Heterojunction Gas Sensors Based on SnO_2-Cr_2O_3 Nanocomposites to H_2 against CO and Its Selectivity Mechanism. *Langmuir* **2021**, *37*, 13548–13558.
15. De la Torre, G.; Vazquez, P.; Agullo-Lopez, F.; Torres, T. Phthalocyanines and related compounds:organic targets for nonlinear optical applications. *J. Mater. Chem.* **1998**, *8*, 1671–1683.
16. Böttger, B.; Schindewolf, U.; Avila, J.L.; Rodrigues-Amaro, R. Catalytic electrodeposition of silver on glassy carbon electrodes modified with films of cobalt phthalocyanine. *J. Electroanal. Chem.* **1997**, *432*, 139–144.
17. Neghabi, M.; Zadsar, M.; Ghorashi, S.M.B. Investigation of structural and optoelectronic properties of annealed nickel phthalocyanine thin films. *Mater. Sci. Semicond. Process.* **2014**, *17*, 13–20.
18. Cho, S.W.; Piper, L.F.J.; DeMasi, A.; Preston, A.R.H.; Smith, K.E.; Chauhan, K.V.; Sullivan, P.; Hatton, R.A.; Jones, T.S. Soft X-ray Spectroscopy of C_{60}/Copper Phthalocyanine/MoO_3 Interfaces: Role of Reduced MoO_3 on Energetic Band Alignment and Improved Performance. *J. Phys. Chem. C* **2010**, *114*, 18252–18257. [CrossRef]
19. El-Nahass, M.M.; Abd-El-Rahman, K.F.; Darwish, A.A.A. Fourier-transform infrared and UV-vis spectroscopes of nickel phthalocyanine thin films. *Mater. Chem. Phys.* **2005**, *92*, 185–189.
20. Yin, X.; Wu, S.; Dastan, D.; Nie, S.; Liu, Y.; Li, Z.; Zhou, Y.; Li, J.; Faik, A.; Shan, K.; et al. Sensing Selectivity of SnO_2-Mn_3O_4 Nanocomposite Sensors for the Detection of H_2 and CO Gases. *Surf. Interfaces* **2021**, *25*, 101190.
21. Klyamer, D.; Sukhikh, A.; Nikolaeva, N.; Morozova, N.; Basova, T. Vanadyl Phthalocyanine Films and Their Hybrid Structures with Pd Nanoparticles: Structure and Sensing Properties. *Sensors* **2020**, *20*, 1893. [CrossRef]
22. Zhou, W.; Dastan, D.; Yin, X.; Nie, S.; Wu, S.; Wang, Q.; Li, J. Optimization of gas sensing properties of n-SnO_2/p-x CuO sensors for homogenous gases and the sensing mechanism. *J. Mater. Sci. Mater. Electron.* **2020**, *31*, 18412–18426. [CrossRef]
23. Sharma, A.K.; Mahajan, A.; Saini, R.; Bedi, R.K.; Kumar, S.; Debnath, A.K.; Aswal, D.K. Reversible and fast responding ppb level Cl_2 sensor based on noncovalent modified carbon nanotubes with Hexadecafluorinated copper phthalocyanine. *Sens. Actuators B Chem.* **2018**, *255*, 87–99. [CrossRef]
24. Shan, K.; Yi, Z.; Yin, X.T.; Dastan, D.; Altaf, F.; Garmestani, H.; Alamgir, F.M. Mixed conductivity evaluation and sensing characteristics of limiting current oxygen sensors. *Surf. Interfaces* **2020**, *21*, 100762. [CrossRef]
25. Liu, Q.; Gao, L.; Su, X.; Zhou, F.; Duan, G. Interfacial self-assembly of CoPc thin films with their high sensing use as NO_2 sensors. *Mater. Chem. Phys.* **2019**, *234*, 94–101. [CrossRef]
26. Xia, S.; Shi, Z.; Sun, L.; Sun, S.; Dastan, D.; Fan, R. Suppressing the loss and enhancing the breakdown strengths of high-k materials via constructing layered structure. *Mater. Lett.* **2022**, *312*, 131654.
27. Ambily, S.; Menon, C.S. The effect of growth parameters on the electrical, optical and structural properties of copper phthalocyanine thin films. *Thin Solid Film.* **1999**, *347*, 284–288.

28. Janczak, J. Temperature dependence on recrystallisation of the magnesium phthalocyanine (MgPc) in triethylamine. *Polyhedron* **2010**, *29*, 941–949. [CrossRef]
29. Kim, I.; Haverinen, H.M.; Wang, Z.; Madakuni, S.; Li, J.; Jabbour, G.E. Effect of molecular packing on interfacial recombination of organic solar cells based on palladium phthalocyanine and perylene derivatives. *Appl. Phys. Lett.* **2009**, *95*, 023305. [CrossRef]
30. Jarosz, G. On small signal capacitance spectra of organic diode formed by ITO-palladium phthalocyanine-Al sandwich system. *Thin Solid Film.* **2010**, *518*, 4015–4018.
31. Gould, R.D. Structure and electrical conduction properties of phthalocyanine thin films. *Coord. Chem. Rev.* **1996**, *156*, 237–274. [CrossRef]
32. De Haan, A.; Debliquy, M.; Decroly, A. Influence of atmospheric pollutants on the conductance of phthalocyanine films. *Sens. Actuators B Chem.* **1999**, *57*, 69–74. [CrossRef]
33. Lasmi, M.; Mahtout, S.; Rabilloud, F. The effect of palladium and platinum doping on the structure, stability and optical properties of germanium clusters: DFT study of $PdGe_n$ and $PtGe_n$ (n = 1–20) clusters. *Comput. Theor. Chem.* **2020**, *1181*, 112830. [CrossRef]
34. Azam, S.; Goumri-Said, S.; Khan, S.; Kanoun, M. Electronic, optical and thermoelectric properties of new metal-rich homological selenides with palladium–indium: Density functional theory and Boltzmann transport model. *J. Phys. Chem. Solids* **2020**, *138*, 109229. [CrossRef]
35. Brahim, H. DFT/TD-DFT investigation on the UV-vis absorption and phosphorescence spectra of platinum (II) and palladium (II) complexeswith Schiff-base ligands. *J. Lumin.* **2019**, *210*, 96–103. [CrossRef]
36. Timoumi, A.; Al Turkestani, M.K.; Alamri, S.N.; Alamri, H.; Ouerfelli, J.; Jamoussi, B. Synthesis and characterization of thin films of palladium (II) phthalocyanine and its derivatives using the thermal evaporation technique. *Mater. Sci. Mater. Electron.* **2017**, *28*, 7480–7488. [CrossRef]
37. Timoumi, A.; Bouguila, N.; Koaib, J.; Al Turkestani, M.K.; Jamoussi, B. Study of electrical and dielectric properties of palladium phthalocyanine (PdPc) in pellet form. *Mater. Res. Express* **2019**, *6*, 055103. [CrossRef]
38. Melville, O.A.; Lessard, B.H.; Bender, T.P. Phthalocyanine-Based Organic Thin-Film Transistors: A Review of Recent Advances. *ACS Appl. Mater. Interfaces* **2015**, *7*, 13105–13118. [CrossRef] [PubMed]
39. Juan, A.; Tejada, J.; Lopez-Varo, P.; Chaure, N.B.; Chambrier, I.; Cammidge, A.N.; Cook, M.J.; Jafari-Fini, A.; Ray, A.K. Organic thin film transistors using a liquid crystalline palladium phthalocyanine as active layer. *J. Appl. Phys.* **2018**, *123*, 115501.
40. Zheng, X.; Wang, Y.; Hu, J.; Yang, G.; Guo, Z.; Xia, J.; Xu, Z.; Fang, G. Octamethyl-substituted Pd(ii) phthalocyanine with long carrier lifetime as a dopant-free hole selective material for performance enhancement of perovskite solar cells. *J. Mater. Chem. A* **2017**, *246*, 24416–24424. [CrossRef]
41. Karl, N.; Kraft, K.H.; Marktanner, J.; Munch, M.; Schatz, F.; Stehle, R.; Uhde, H.M.; Vac, J. Fast electronic transport in organic molecular solids? *Sci. Technol. A* **1999**, *17*, 2318–2328. [CrossRef]
42. Xu, J.; Zhao, L.; Hou, W.; Guo, H.; Zhang, H. Dependence of morphology, substrate and thickness of iron phthalocyanine thin films on the photocatalytic degradation of rhodamine B dye. *Chem. Pap.* **2018**, *72*, 2327–2337. [CrossRef]
43. Chakane, S.; Datir, A.; Koinkar, P. Spin coated unsubstituted copper phthalocyanine thin films for nitrogen dioxide sensors. *Mod. Phys. Lett. B* **2015**, *29*, 1540032. [CrossRef]
44. Al-Raqa, S.Y.; Solieman, A.S.; Joraid, A.A.; Alamri, S.N.; Moussa, Z.; Aljuhani, A. Preparation and optical properties of novel symmetrical hexadecachlorinatedphthalocyaninato zinc (II) spin coated thin films. *Polyhedron* **2008**, *27*, 1256–1261. [CrossRef]
45. Critchley, S.M.; Willis, M.R. Deposition of thin phthalocyanine films by spin coating. *Int. J. Electron.* **1994**, *76*, 809–814. [CrossRef]
46. Jafari, M.J.; Azim-Araghi, M.E.; Barhemat, S. Effect of chemical environments on palladium phthalocyanine thin film sensors for humidity analysis. *J. Mater. Sci.* **2012**, *47*, 1992–1999. [CrossRef]
47. Mphuthi, N.G.; Adekunle, A.S.; Fayemi, O.E.; Olasunkanmi, L.O.; Ebenso, E.E. Phthalocyanine Doped Metal Oxide Nanoparticles on Multiwalled Carbon Nanotubes Platform for the detection of Dopamine. *Sci. Rep.* **2017**, *7*, 1–23. [CrossRef]
48. Silva, J.; Sekhar, K.; Negrea, R.; Ghica, C.; Dastan, D.; Gomes, M. Ferroelectric properties of ZrO_2 films deposited on ITO-coated glass. *Ceram. Int.* **2022**, *48*, 6131–6137. [CrossRef]
49. Chu, Q.; Sun, Z.; Liu, Y.; Cui, H.; Cheng, B.; Dastan, D.; Moon, K.; Yang, G.; Wong, C. Difluorobenzylamine Treatment of Organolead Halide Perovskite Boosting High Efficiency and Stable Photovoltaic Cells. *ACS Appl. Mater. Interfaces* **2022**, *14*, 11388–11397. [CrossRef]
50. Lokesh, K.S.; Adriaens, A. Synthesis and characterization of tetra-substituted palladium phthalocyanine complexes. *Dye. Pigment.* **2013**, *96*, 269–277. [CrossRef]
51. Mohammed, M.; Al-Mousoi, A.; Singh, S.; Younis, U.; Kumar, A.; Dastan, D.; Ravi, G. Ionic Liquid Passivator for Mesoporous Titanium Dioxide Electron Transport Layer to Enhance Efficiency and Stability of Hole Conductor-Free Perovskite Solar Cells. *Energy Fuels* **2022**. [CrossRef]
52. Mohammad Beigia, S.; Mesgari, F.; Hossein, M.; Dastan, D.; Xu, G. Electrochemiluminescence Sensors based on Lanthanide Nanomaterials as Modifiers. *Curr. Anal. Chem.* **2022**, *18*, 53–62. [CrossRef]
53. Borker, P.; Salker, A.V.J. Synthesis, characterization and photocatalytic studies of some metal phthalocyanines. *Chem. Tech.* **2006**, *13*, 341.
54. Seoudi, R.; El-Bahy, G.S.; El Sayed, Z.A. Ultraviolet and visible spectroscopic studies of phthalocyanine and its complexes thin films. *Opt. Mater.* **2016**, *29*, 304–312. [CrossRef]

55. Sumimoto, M.; Honda, T.; Kawashima, Y.; Hori, K.; Fujimoto, H. Theoretical and experimental investigation on the electronic properties of the shuttlecock shaped and the double-decker structured metal phthalocyanines, MPc and $M(Pc)_2$ (M = Sn and Pb). *Dalton Trans.* **2012**, *23*, 7141–7150. [CrossRef]
56. Tao, L.; Huang, J.; Dastan, D.; Wang, T.; Li, J.; Yin, X.; Wang, Q. New insight into absorption characteristics of CO_2 on the surface of calcite, dolomite, and magnesite. *Appl. Surf. Sci.* **2021**, *540*, 148320. [CrossRef]
57. Toader, M.; Hietschold, M. Tuning the energy level alignment at the SnPc/Ag (111) interface using an STM tip. *J. Phys. Chem. C* **2011**, *115*, 3099–3105. [CrossRef]
58. Tao, L.; Huang, J.; Dastan, D.; Li, J.; Yin, X.; Wang, Q. Flue Gas Separation at Organic-Inorganic Interface under Geological Conditions. *Surf. Interfaces* **2011**, *27*, 101462. [CrossRef]
59. Sumimoto, M.; Honda, T.; Kawashima, Y.; Horia, K.; Fujimoto, H. Significance of dimer models describing physical properties in a triclinic solid of tin(ii) phthalocyanine. *RSC Adv.* **2012**, *33*, 12798–12803. [CrossRef]
60. Ţălu, Ş.; Kulesza, S.; Bramowicz, M.; Stępień, K.; Dastan, D. Analysis of the Surface Microtexture of Sputtered Indium Tin Oxide Thin Films. *Arch. Metall. Mater.* **2021**, *66*, 443.
61. Timoumi, A.; Albetran, H.M.; Alamri, H.R.; Alamri, S.N.; Low, I.M. Impact of annealing temperature on structural, morphological and optical properties of GO-TiO_2 thin films prepared by spin coating technique. *Superlattices Microstruct.* **2020**, *139*, 106423. [CrossRef]
62. Timoumi, A.; Bouzouita, H.; Kanzari, M.; Rezig, B. Fabrication and characterization of In_2S_3 thin films deposited by thermal evaporation technique. *Thin Solid Film.* **2005**, *480*, 124–128. [CrossRef]
63. Timoumi, A.; Bouzouita, H.; Rezig, B. Optical constants of Na–In_2S_3 thin films prepared by vacuum thermal evaporation technique. *Thin Solid Film.* **2011**, *519*, 7615–7619. [CrossRef]
64. Dastan, D.; Shan, K.; Jafari, A.; Gity, F.; Yin, X.; Shi, Z.; Alharbi, N.; Reshi, B.; Fu, W.; Ţălu, Ş.; et al. Influence of nitrogen concentration on electrical, mechanical, and structural properties of tantalum nitride thin films prepared via DC magnetron sputtering. *Appl. Phys. A* **2022**, *128*, 400. [CrossRef]
65. Yin, X.; Huang, H.; Xie, J.; Dastan, D.; Li, J.; Liu, Y.; Tan, X.; Gao, X.; Shah, W.; Ma, X. High-performance visible-light active Sr-doped porous $LaFeO_3$ semiconductor prepared via sol-gel method. *Green Chem. Lett. Rev.* **2022**, *15*, 546–556. [CrossRef]
66. Frisch, M.J. Gaussian 09, Revision D. 2016; 1.
67. Liu, L.; Sheng, Y.Y.; Liu, M.; Dienwiebel, M.; Zhang, Z.; Dastan, D. Formation of the third bodies of steel sliding against brass under lubricated conditions. *Tribol. Int.* **2019**, *140*, 105727. [CrossRef]
68. Grimme, S.; Antony, J.; Ehrlich, S.; Krieg, H. A consistent and accurate ab initio parametrization of density functional dispersion correction (DFT-D) for the 94 elements H-Pu. *J. Chem. Phys.* **2010**, *132*, 154104. [CrossRef] [PubMed]
69. Fuentealba, P.; Preuss, H.; Stoll, H.; Von Szentpály, L. A proper account of core-polarization with pseudopotentials: Single valence-electron alkali compounds. *Chem. Phys. Lett.* **1982**, *89*, 418–422. [CrossRef]
70. Marenich, A.V.; Cramer, C.J.; Truhlar, D.G. Universal Solvation Model Based on Solute Electron Density and on a Continuum Model of the Solvent Defined by the Bulk Dielectric Constant and Atomic Surface Tensions. *J. Phys. Chem. B* **2009**, *113*, 6378–6396. [CrossRef]
71. Fleming, I. *Frontier Orbitals and Organic Chemical Reactions*; John Wiley & Sons, Ltd.: London, UK, 1982; Volume 879.
72. Kavitha, E.; Sandaraganesan, N.; Sebastian, S. Molecular structure, vibrational spectroscopic and HOMO, LUMO studies of 4-nitroaniline by density functional method. *Indian J. Pure Appl. Phys.* **2010**, *48*, 20.
73. Zainuri, D.A.; Razak, I.A.; Arshad, S. Crystal structures, DFT studies and UV–visible absorption spectra of two anthracenyl chalcone derivatives. *Acta Cryst. E* **2018**, *74*, 1491–1496. [CrossRef]
74. Lisi, S.; Gargiani, P.; Scardamaglia, M.; Brookes, N.B.; Sessi, V.; Mariani, C.; Betti, M.G. Graphene-Induced Magnetic Anisotropy of a Two-Dimensional Iron Phthalocyanine Network. *J. Phys. Chem. Lett.* **2015**, *6*, 1690–1695. [CrossRef]
75. Bufon, C.C.B.; Vervacke, C.; Thurmer, D.J.; Fronk, M.; Salvan, G.; Lindner, S.; Knupfer, M.; Zahn, D.R.T.; Schmidt, O.G. Determination of the Charge Transport Mechanisms in Ultrathin Copper Phthalocyanine Vertical Heterojunctions. *J. Phys. Chem. C* **2014**, *118*, 7272–7279. [CrossRef]
76. Skoog, D.A.; Holler, F.J.; Crouch, S.R. *Principles of Instrumental Analysis*; Cengage Learning: Boston, MA, USA, 2017; Volume 335.
77. Davidson, A.T. The effect of the meal atom on the absorption spectra of phthalocyanine films. *J. Chem. Phys.* **1982**, *77*, 168–172. [CrossRef]
78. Martínez-Bourget, D.; Rocha, E.; Labra-Vázquez, P.; Santillan, R.; Ortiz-López, B.; Ortiz-Navarrete, V.; Maraval, V.; Chauvin, R.; Farfán, N. BODIPY-Ethynylestradiol molecular rotors as fluorescent viscosity probes in endoplasmic reticulum. *Spectrochim. Acta A Mol. Biomol. Spectrosc.* **2022**, *283*, 121704. [CrossRef]
79. Haghnegahdar, N.; AbbasiTarighat, M.; Dastan, D. Curcumin-functionalized nanocomposite AgNPs/SDS/MWCNTs for electrocatalytic simultaneous determination of dopamine, uric acid, and guanine in co-existence of ascorbic acid by glassy carbon electrode. *J. Mater. Sci. Mater. Electron.* **2021**, *32*, 5602–5613. [CrossRef]
80. Zhang, M.; Shi, Z.; Zhang, J.; Zhang, K.; Lei, L.; Dastan, D.; Dong, B. Greatly Enhanced Dielectric Charge Storage Capabilities of Layered Polymer Composites Incorporated with low loading fractions of Ultrathin Amorphous Iron Phosphate Nanosheets. *J. Mater. Chem. C* **2021**, *9*, 10414–10424. [CrossRef]
81. Kartha, M.; Reshi, B.; Walke, P.; Dastan, D. Morphological Study of Thin Films: Simulation and Experimental Insights using Horizontal Visibility Graph. *Ceram. Int.* **2022**, *48*, 5066–5074. [CrossRef]

82. Abbasi, S.; Dastan, D.; Ţălu, Ş.; Tahir, M.; Elias, M.; Tao, L.; Li, Z. Evaluation of the dependence of methyl orange organic pollutant removal rate on the amount of titanium dioxide nanoparticles in MWCNTs-TiO_2 photocatalyst using statistical methods and Duncan's multiple range test. *Int. J. Environ. An. Chem.* **2022**, 1–15. [CrossRef]
83. Timoumi, A.; Zayoud, W.; Sharma, A.; Kraini, M.; Bouguila, N.; Hakamy, A.; Revaprasadu, N.; Alaya, S. Impact of thermal annealing inducing oxidation processon the crystalline powder of In_2S_3. *J. Mater. Sci. Mater. Electron.* **2020**, *31*, 13636–13645. [CrossRef]
84. Liang, L.; Shi, Z.; Tan, X.; Sun, S.; Chen, M.; Dastan, D.; Dong, B.; Cao, L. Largely Improved Breakdown Strength and Discharge Efficiency of Layer-Structured Nanocomposites by Filling with a Small Loading Fraction of 2D Zirconium Phosphate Nanosheets. *Adv. Mater. Interfaces* **2022**, 2101646. [CrossRef]
85. Asadzadeh, M.; Tajabadi, F.; Dastan, D.; Sangpour, P.; Shi, Z.; Taghavinia, N. Facile deposition of porous fluorine doped tin oxide by Dr. Blade method for capacitive applications. *Ceram. Int.* **2021**, *47*, 5487–5494. [CrossRef]
86. El-Nhass, M.M.; Solman, H.S.; Metwally, H.S.; Farid, A.M.; Farag, A.A.M.; El Shazly, A.A. Optical properties of evaporated iron phthalocyanine (FePc) thin films. *J. Opti.* **2001**, *30*, 121–129. [CrossRef]
87. Kim, H.J.; Kim, J.W.; Lee, H.H.; Lee, B.; Kim, J.-J. Initial growth mode, nanostructure, and molecular stacking of a ZnPc:C60 bulk heterojunction. *Adv. Funct. Mater.* **2012**, *22*, 4244–4248. [CrossRef]